



Semnan University

Mechanics of Advanced Composite Structures

journal homepage: <http://MACS.journals.semnan.ac.ir>

Frequency Analysis of Functionally Graded Carbon Nanotube-reinforced Cylindrical Panels by Mesh-free Galerkin Method

J. Alihemmati^a, Y. Tadi Beni^{b,c*}, A. Soltanmaleki^d, M. Nejati^d

^a Mechanical Engineering Department, Shahrekord University, Shahrekord, Iran

^b Faculty of Engineering, Shahrekord University, Shahrekord, Iran.

^c Nanotechnology Research Center, Shahrekord University, 8818634141, Shahrekord, Iran

^d Faculty of Mechanical Engineering, Semnan University, Semnan, Iran

KEYWORDS

Free vibration
Carbon nanotube-reinforced composite
Mesh-free method

ABSTRACT

In this work, the three-dimensional mesh-free (3D-Mfree) method is used for free vibration analysis of functionally graded (FG) cylindrical panels reinforced by carbon nanotubes. The material properties of panels are considered to be changed linearly in the thickness direction, and the effective material properties of the panels are estimated by the rule of mixture. Five models of carbon nanotubes distribution, including a uniform distributed model and four FG distributed models, are considered. The weak form governing equations of motion are derived using Hamilton's principle, and the moving least squares (MLS) approximation is used to construct the 3D-Mfree shape functions in cylindrical coordinates. Various boundary conditions are considered, and effects of boundary conditions, carbon nanotube distribution, the volume fraction of carbon nanotubes, and the panel geometry on the natural frequencies are studied. The results are compared with other results available in the literature, and a close agreement is observed.

1. Introduction

Carbon nanotubes (CNTs) have been widely accepted because of their many mechanical, electrical, and thermal properties and now attracted more attention in engineering applications. Usually, stiff fillers reinforce ordinary composites with macro-scale dimensions embedded in a variety of matrixes to improve the mechanical property of the composite system. The discovery of CNTs changed the traditional macro-scale filler reinforcements by newly discovered nanoscale reinforcements [1].

Recently, CNTs were considered for use as reinforcements in modern composite structures because of their high elastic properties and strength compared to conventional fibers. For example, Young's modulus of a CNT is higher than 1 TPa, and its tensile strength is about 150 GPa; it means that they are a hundred times stronger than steel, whereas they are three to five times lighter than it. Some advantages make carbon nanotube-reinforced composite used in many

structures designed to undergo high mechanical and thermal loads with low weight [2].

Many researchers studied the vibration of conventional composites, but a few studies have utilized the vibration of carbon nanotube reinforced composites (CNTRCs); on the other hand, most of the research deals with the mechanical and thermal properties of CNTRCs. Some research about the vibration of CNTRCs is as follows:

The nonlinear bending analysis of plates made of carbon nanotube-reinforced composite was studied by Shen [3]. In this work, the mechanical properties of carbon nanotubes were considered dependent on temperature, and the molecular dynamics simulation was used to compute the mechanical properties. Ke et al. [4] performed nonlinear free vibration analysis of functionally graded carbon nanotube-reinforced composite beams. Their work is based on the Timoshenko beam theory, and the von Kármán geometric nonlinearity is considered. They assume that the mechanical property of carbon nanotube-reinforced composite beams are varied in thickness direction based on the rule of the

* Corresponding author. Tel.: +98-9126385016
E-mail address: tadi@sku.ac.ir

mixture, and finally, the Ritz method is used to extract the governing equations. Vibration behavior analysis of functionally graded carbon nanotube-reinforced cylindrical panels was studied by Sobhani Aragh et al. [5]. The effective mechanical properties of the composite are derived with Eshelby–Mori–Tanaka's approach and the two-dimensional generalized differential quadrature method (GDQM) was used to solve the governing equations and apply the corresponding boundary conditions. Wang and Shen [6] studied the nonlinear bending and vibration analysis of a sandwich plate; the sandwich plate was made of carbon nanotube-reinforced composite face sheets, and their mechanical properties change along the thickness direction. Dynamic investigation of nanocomposite cylinders reinforced by single-walled carbon nanotubes through the Mfree method conducted by Moradi-Dastjerdi et al. [7]. They used moving least squares (MLSs) shape functions to approximate the displacement field in an axisymmetric model. Lin and Xiang [8] studied free vibration analysis of carbon nanotube-reinforced composite beams based on the first and third-order beam theories. They used both uniform and functionally graded distribution of carbon nanotube reinforcement. The Ritz method was employed to extract the natural frequencies, and they concluded that FGX-CNT beams in all conditions exhibit the highest natural frequencies, and the beams with the FG_CNT model of reinforcements give the lowest natural frequencies. Free vibration analysis of carbon nanotube-reinforced polymer composite structures with various geometries is carried out by Mehar et al. [9]. They used a generic higher-order shear deformation theory, and Hamilton's principle derives the equations of motion of the structures, and finally, the solution of equations was performed by the finite-element method. Karami et al. [10] presented an analytical study on functionally graded carbon nanotube-reinforced composite plates. Their work is based on second-order shear deformation theory, and also they included the size effects with nonlocal elasticity theory in their analysis. Vibration analysis of FG-CNTRC in different geometries such as circular, annular, and sector plates is studied by Zhon et al. [11]. First-order shear deformation theory was used, and then the natural frequencies and corresponding mode shapes were extracted by the Ritz-variational method. The free vibration frequency of composite plates reinforced with single-walled carbon nanotubes by using a refined simplified two-variable n th-higher-order theory is performed by Bouazza and Zenkour [12]. They used an exact closed-form formulation based on this theory for solving the equations.

Bending analysis of nano/microbeams under the concentrated and distributed loads is investigated by Demir and Civalek [13]. They used Euler Bernoulli beam theory via the enhanced Eringen differential model. Also, the singularity function method is used to calculate the deflection of the concentrated and distributed loaded beams.

Dynamic instability of viscoelastic porous functionally graded nanobeam embedded on visco-Pasternak medium subjected to an axially oscillating loading and the magnetic field is performed by Jalaei and Civalek [14]. They employed Eringen's differential law in conjunction with Timoshenko beam theory and Hamilton's principle to derive equations of motion. Finally, Navier's solution and Bolotin's approach are utilized to obtain the dynamic instability region of viscoelastic porous FG nanobeam.

Civalek et al. [15] studied free vibration analysis of carbon nanotube-reinforced composite microbeams. In their work, carbon nanotubes are distributed in a polymeric matrix with four different reinforcement patterns, and material properties of the CNTRC microbeams are predicted by using the rule of mixture. Hamilton's principle derives the microstructure-dependent governing differential equations based on the couple stress theory. Finally, the obtained vibration equation is solved by using Navier's solution method.

Buckling and free vibration of rectangular polymeric laminate reinforced by graphene sheets are investigated by Karimi Zeverdejani and Tadi Beni [16]. In this paper, various patterns are considered for the augmentation of each laminate. Critical buckling load is evaluated for different parameters, including boundary conditions, reinforcement pattern, loading regime, and laminate geometric states.

Buckling and post-buckling of graphene-reinforced laminated composite plates subjected to uniaxial and biaxial loadings are investigated by Karimi Zeverdejani et al. [17]. This paper uses poly-methyl-methacrylate for the matrix, and three patterns are considered for the plate cross-section. Graphene sheets are considered in both perfect and defective forms. The free vibration of polymer nanocomposite reinforced by graphene sheet is investigated by Karimi Zeverdejani and Tadi Beni [18]. In this work, the new size-dependent formulation is presented for nanocomposites based on the couple stress theory. For this purpose, the first shear deformation theory is applied. The effect of the scale parameter is investigated based on anisotropic couple stress theory. It is observed that graphene defects cause to diminish the lamina frequency.

Three-dimensional (3D) vibration analysis of FG carbon nanotube reinforced cylindrical panel with the mesh-free method has not been studied to the best of the authors' knowledge. Also, there are two main shortcomings and limitations in many works performed before: two-dimensional modeling using shell theories and limitations in modeling boundary conditions. So the major aim of the present work is a three-dimensional free vibration study of FG carbon nanotube reinforced cylindrical panels under various boundary conditions using the Mfree method. The volume fraction of carbon nanotubes, the geometry of the panel, and boundary conditions are the parameters that their effects on natural frequencies are studied in this paper. For validation of the 3D-Mfree approach, the results were compared with the available results in the literature for various material properties such as homogeneous, isotropic, and fiber-reinforced cylindrical panels.

2. Statement of the Problem

2.1. The material properties of CNTs

A carbon nanotube reinforced cylindrical panel of radius R_a , with dimension $L \times S$, different boundary conditions at the edges $\theta = 0, \theta = \alpha$ and Also at the edges $z = 0, z = L$ is shown in Fig. 1. The effective mechanical property of CNTRC cylindrical panels are obtained as [7,19]

$$E_{11} = \eta_1 V_{CN} E_{11}^{CN} + V_m E^m, \quad \frac{\eta_2}{E_{22}} = \frac{V_{CN}}{E_{22}^{CN}} + \frac{V_m}{E^m}$$

$$E_{33} = E_{22}, \quad \frac{\eta_3}{G_{12}} = \frac{V_{CN}}{G_{12}^{CN}} + \frac{V_m}{G^m} \tag{1}$$

$$v_{ij} = V_{CN} v_{ij}^{CN} + V_m v^m, \quad \rho = V_{CN} \rho^{CN} + V_m \rho^m$$

where, $E_{11}^{CN}, E_{22}^{CN}, G_{12}^{CN}, v_{ij}^{CN}$ and ρ^{CN} are elasticity modules, shear module, Poisson's ratio and mass density of CNTs, respectively and E^m, G^m, v^m and ρ^m are those of matrix respectively. η_j ($j = 1, 2, 3$) are the CNTs efficiency that determined by matching the elastic modulus of CNTRCs obtained by the MD simulation results with the numerical results are obtained from the rule of mixture.

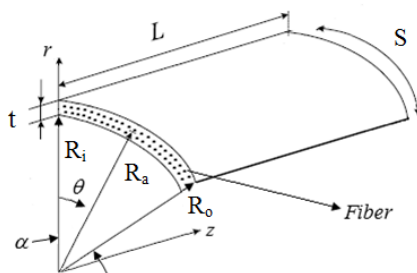


Fig. 1. The design scheme of the CNTRC cylindrical panels

Furthermore, V_m are CNTs and matrix volume fractions and defined as:

$$V_m + V_{CN} = 1 \tag{2}$$

Five profiles of linear variation of CNTs volume fraction in the thickness direction are considered (Fig. 2) and defined as:

1. Uniform distributed (UD)

$$V_{CN} = V_{CN}^* \tag{3}$$

2. FG-V

$$V_{CN} = 2 \left(\frac{r-a}{h} \right) V_{CN}^* \tag{4}$$

3. FG-Λ

$$V_{CN} = 2 \left(\frac{b-r}{h} \right) V_{CN}^* \tag{5}$$

4. FG-X

$$V_{CN} = 4 \left| \frac{r-R_m}{h} \right| V_{CN}^* \tag{6}$$

5. FG-ϕ

$$V_{CN} = 4 \left(0.5 - \left| \frac{r-R_m}{h} \right| \right) V_{CN}^* \tag{7}$$

where

$$V_{CN}^* = \frac{\rho^m}{w^{CN} + (\rho^{CN} / w^{CN}) - \rho^{CN}} \tag{8}$$

where, w^{CN} is the mass fraction of CNTs.

The Poisson's ratio is considered to change according to reference [3], i.e.

$$v_{12} = V_{CN}^* v_{12}^{CN} + V_m v^m \tag{9}$$

2.2. Governing equations

Hamilton's principle is used for extracting the weak forms of governing equations. In the absence of external works, Hamilton's principle for free vibration analysis is indicated as below [20]:

$$\delta \int_{t_1}^{t_2} (T - \Pi) dt = 0 \tag{10}$$

where T is kinetic energy, Π refers to elastic strain energy. More in detail, as follows:

$$T = \frac{1}{2} \int_{\Omega} \rho \dot{u}^T \dot{u} dv \tag{11}$$

$$\Pi = \frac{1}{2} \int_{\Omega} \epsilon^T \sigma dv \tag{12}$$

In the above relations, $\sigma, \epsilon, u, \dot{u}$, and ρ are stress vector, strain vector, displacement vector, velocity vector, and mass density, respectively. Also Ω is the whole volume of the continuum body. Using Eqs. (11) and (12), in Eq. (10), the equation of motion can be expressed as weak form by the following relation:

$$\int_{\Omega} \delta \epsilon^T \sigma dv + \int_{\Omega} \rho \delta u^T \ddot{u} dv = 0 \tag{13}$$

in which, \ddot{u} is acceleration vector.

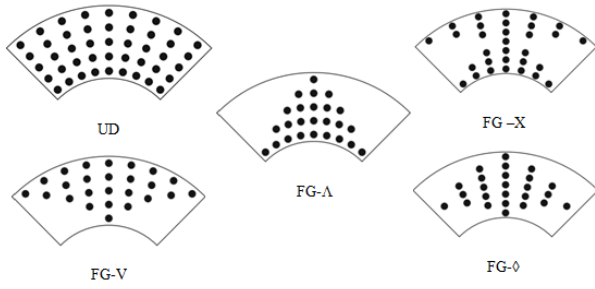


Fig. 2. Five profiles of linear variation of CNTs volume fraction in the thickness direction

For a linear elastic body, the general Hook’s law is defined as follow:

$$\sigma = D\varepsilon \tag{14}$$

where D for an orthotropic body [20] is as follows:

$$D = \begin{bmatrix} C_{11} & C_{12} & C_{13} & 0 & 0 & 0 \\ C_{12} & C_{22} & C_{23} & 0 & 0 & 0 \\ C_{13} & C_{23} & C_{33} & 0 & 0 & 0 \\ 0 & 0 & 0 & C_{44} & 0 & 0 \\ 0 & 0 & 0 & 0 & C_{55} & 0 \\ 0 & 0 & 0 & 0 & 0 & C_{66} \end{bmatrix} \tag{15}$$

In which:

$$\begin{aligned} C_{11} &= E_1 \frac{1-\nu_{23}\nu_{32}}{\Delta} & C_{12} &= E_1 \frac{\nu_{21} + \nu_{31}\nu_{23}}{\Delta} \\ C_{13} &= E_1 \frac{\nu_{31} + \nu_{21}\nu_{32}}{\Delta} & C_{22} &= E_2 \frac{1-\nu_{31}\nu_{13}}{\Delta} \\ C_{23} &= E_2 \frac{\nu_{32} + \nu_{12}\nu_{31}}{\Delta} & C_{33} &= E_3 \frac{1-\nu_{21}\nu_{12}}{\Delta} \\ C_{44} &= G_{23} & C_{55} &= G_{31} & C_{66} &= G_{12} \\ \Delta &= 1 - \nu_{32}\nu_{23} - \nu_{21}\nu_{12} - \nu_{13}\nu_{31} - 2\nu_{32}\nu_{21}\nu_{13} \end{aligned} \tag{16}$$

Stress and strain vectors in cylindrical coordinates are as follows:

$$\begin{aligned} \sigma &= [\sigma_z \quad \sigma_\theta \quad \sigma_r \quad \sigma_{r\theta} \quad \sigma_{rz} \quad \sigma_{\theta z}]^T \\ \varepsilon &= [\varepsilon_z \quad \varepsilon_\theta \quad \varepsilon_r \quad \varepsilon_{r\theta} \quad \varepsilon_{rz} \quad \varepsilon_{\theta z}]^T \end{aligned} \tag{17}$$

3. Mesh-free Formulation

The mesh-free Galerkin method based on moving least squares approximation (MLS) is used in this work. In this method, the field variable $u(\mathbf{X})$ in the domain Ω at an arbitrary point $\mathbf{X}(r, \theta, z)$ in the cylindrical coordinate is approximated as follows [21, 22, 23]:

$$u(X) = \sum_{i=1}^m P_i(X)a_i = P^T(X)a(X) \tag{18}$$

where $\mathbf{P}(\mathbf{X})$, $\mathbf{a}(\mathbf{X})$ and m are the base vector, the variable coefficients vector, and the number of components of the base vector, respectively. In 3D space in cylindrical coordinate, a complete base vector basis of order s is given by:

$$P(X) = [1 \quad r \quad \theta \quad zr\theta \quad \theta z \quad rz \quad r^2 \quad \theta^2 \quad z^2 \quad \dots \quad r^s \quad \theta^s \quad z^s]^T \tag{19}$$

Furthermore, $\mathbf{a}(\mathbf{X})$ is a general function that, in MLS approximation, at an arbitrary point \mathbf{X} , $\mathbf{a}(\mathbf{X})$ is considered to minimize the weighted residual.

The weighted residual is defined as:

$$J = \sum_{i=1}^n w(X - X_i)[P^T(X)a(X) - \hat{u}_i]^2 \tag{20}$$

in which, n , $w(\mathbf{X} - \mathbf{X}_i)$ and \hat{u}_i are the number of nodes in the support domain of the point $\mathbf{X}(r, \theta, z)$, the weight function, and virtual nodal value at the node \mathbf{X}_i , respectively. By minimization the weighted residual:

$$\frac{\partial J}{\partial \mathbf{a}} = 0 \tag{21}$$

$\mathbf{a}(\mathbf{X})$ is derived as follow:

$$a(X) = [M(X)]^{-1}Q(X)\hat{u} \tag{22}$$

where \mathbf{M} is called the moment matrix given by:

$$M(X) = \sum_{i=1}^n w(X - X_i)P(X_i)P^T(X_i) \tag{23}$$

and

$$\begin{aligned} Q(X) &= [Q_1 \quad Q_2 \quad \dots \quad Q_n] \\ Q_i &= w(X - X_i)P(X_i) \end{aligned} \tag{24}$$

\hat{u} is virtual nodal value vector and defined as follow:

$$\hat{u} = [\hat{u}_1 \quad \hat{u}_2 \quad \dots \quad \hat{u}_n]^T \tag{25}$$

By substituting Eq. (22) in Eq. (18), we have:

$$u(\mathbf{X}) = \sum_{i=1}^n \Phi_i \hat{u}_i \tag{26}$$

Φ_i is MLS shape function of node located at $X = X_i$ and expressed as follow:

$$\Phi_i(X) = P^T(X)[M(X)]^{-1}Q_i \tag{27}$$

Now by using the MLS approximation, the displacement vector \mathbf{u} in cylindrical coordinates can be approximated as follows:

$$u = [u_r \quad u_\theta \quad u_z]^T = \Phi \hat{u} \tag{28}$$

where:

$$\hat{u} = [\hat{u}_r^1 \quad \hat{u}_\theta^1 \quad \hat{u}_z^1 \quad \dots \quad \hat{u}_r^n \quad \hat{u}_\theta^n \quad \hat{u}_z^n]^T \tag{29}$$

and

$$\Phi = \begin{bmatrix} \Phi_1 & 0 & 0 & \Phi_2 & 0 & 0 & \dots & \Phi_n & 0 & 0 \\ 0 & \Phi_1 & 0 & 0 & \Phi_2 & 0 & \dots & 0 & \Phi_n & 0 \\ 0 & 0 & \Phi_1 & 0 & 0 & \Phi_2 & \dots & 0 & 0 & \Phi_n \end{bmatrix} \tag{30}$$

The strain-displacement relationship is expressed in the matrix form as:

$$\varepsilon = B\hat{u} \tag{31}$$

in which \mathbf{B} , the strain matrix is given as:

$$\mathbf{B} = \begin{bmatrix} 0 & 0 & \frac{\partial \Phi_1}{\partial z} & 0 & \dots & 0 & \frac{\partial \Phi_n}{\partial z} \\ \frac{\Phi_1}{r} & \frac{1}{r} \frac{\partial \Phi_1}{\partial \theta} & 0 & \frac{\Phi_2}{r} & \dots & \frac{1}{r} \frac{\partial \Phi_n}{\partial \theta} & 0 \\ \frac{\partial \Phi_1}{\partial r} & 0 & 0 & \frac{\partial \Phi_2}{\partial r} & \dots & 0 & 0 \\ \frac{1}{r} \frac{\partial \Phi_1}{\partial \theta} & \frac{\partial \Phi_1}{\partial r} - \frac{\Phi_1}{r} & 0 & \frac{1}{r} \frac{\partial \Phi_2}{\partial \theta} & \dots & \frac{\partial \Phi_n}{\partial r} - \frac{\Phi_n}{r} & 0 \\ \frac{\partial \Phi_1}{\partial z} & 0 & \frac{\partial \Phi_1}{\partial r} & \frac{\partial \Phi_2}{\partial z} & \dots & 0 & \frac{\partial \Phi_n}{\partial r} \\ 0 & \frac{\partial \Phi_1}{\partial z} & \frac{1}{r} \frac{\partial \Phi_1}{\partial \theta} & 0 & \dots & \frac{\partial \Phi_n}{\partial z} & \frac{1}{r} \frac{\partial \Phi_n}{\partial \theta} \end{bmatrix} \quad (32)$$

In the absence of body forces and surface tractions, using Eqs. (13), (28), and (31) in Eq. (14) leads to:

$$\delta(\hat{\mathbf{u}})^T \left(\int_{\Lambda} B^T DB dv \right) \hat{\mathbf{u}} + \delta(\hat{\mathbf{u}})^T \left(\int_{\Lambda} \rho \Phi^T \Phi dv \right) \hat{\mathbf{u}} = 0 \quad (33)$$

Equation (33) should be satisfied for every arbitrary $\delta(\hat{\mathbf{u}})$. Therefore, we have:

$$\left(\int_{\Lambda} B^T DB dv \right) \hat{\mathbf{u}} + \left(\int_{\Lambda} \rho \Phi^T \Phi dv \right) \hat{\mathbf{u}} = 0 \quad (34)$$

or

$$\hat{\mathbf{M}} \hat{\mathbf{U}} + \hat{\mathbf{K}} \hat{\mathbf{U}} = 0 \quad (35)$$

where:

$$\hat{\mathbf{U}} = [\hat{u}_r^1 \quad \hat{u}_\theta^1 \quad \hat{u}_z^1 \quad \dots \quad \hat{u}_r^N \quad \hat{u}_\theta^N \quad \hat{u}_z^N]^T \quad (36)$$

and

$$\hat{\mathbf{M}} = \int_{\Lambda} \rho \Phi^T \Phi dv \quad , \quad \hat{\mathbf{K}} = \int_{\Lambda} B^T DB dv \quad (37)$$

N is the total number of nodes. Both of these integrals can be obtained simply by numerical

integration. For numerical integration, the panel domain is first discretized by several cells, and the Gauss integration scheme is used for each cell; finally, the global stiffness matrix $\hat{\mathbf{K}}$ and the mass matrix $\hat{\mathbf{M}}$ are obtained numerically by sweeping all gauss integration points inside the domain Ω . For performing the Gauss integration, each cell is mapped into a reference cell with pre-appreciated Gauss integration points and their corresponding weights. By mapping relations, the corresponding Gauss integration points in the cell of the real domain are derived, and integration is performed using the mapped Gauss integration points.

For imposing the essential boundary conditions, the global stiffness and mass matrixes are modified by transformation method as follow:

$$\mathbf{M} = (\mathbf{T}^{-1})^T \hat{\mathbf{M}} \mathbf{T}^{-1} \quad , \quad \mathbf{K} = (\mathbf{T}^{-1})^T \hat{\mathbf{K}} \mathbf{T}^{-1} \quad (38)$$

in which

$$\mathbf{T} = \begin{bmatrix} \Phi_1(\mathbf{X}_1) & 0 & 0 & \dots & \Phi_N(\mathbf{X}_1) & 0 & 0 \\ 0 & \Phi_1(\mathbf{X}_1) & 0 & \dots & 0 & \Phi_N(\mathbf{X}_1) & 0 \\ 0 & 0 & \Phi_1(\mathbf{X}_1) & \dots & 0 & 0 & \Phi_N(\mathbf{X}_1) \\ \vdots & \vdots & \vdots & \dots & \vdots & \vdots & \vdots \\ \Phi_1(\mathbf{X}_N) & 0 & 0 & \dots & \Phi_N(\mathbf{X}_N) & 0 & 0 \\ 0 & \Phi_1(\mathbf{X}_N) & 0 & \dots & 0 & \Phi_N(\mathbf{X}_N) & 0 \\ 0 & 0 & \Phi_1(\mathbf{X}_N) & \dots & 0 & 0 & \Phi_N(\mathbf{X}_N) \end{bmatrix} \quad (39)$$

After modification of stiffness and mass matrixes, the essential boundary conditions are enforced on the modified matrixes exactly like the finite element method. In the modified stiffness and mass matrixes, the row and columns corresponding to the degree of freedoms are removed that we want to be constrained.

4. Validation

In this section, the convergence results are obtained to find the sufficient node numbers and

distribution in the problem domain and its boundaries for extracting the natural frequencies. So, the fundamental natural frequency parameter for a homogeneous isotropic cylindrical panel with (SSSS) boundary conditions and various geometrical parameters is computed and shown in Table 1.

Normalized fundamental frequencies ($\bar{\Omega} = \Omega h \sqrt{\rho_0/E_0}$) for an isotropic FGM cylindrical panel ($L/R_a=0.5, L/t=2$) for various values of power-law index n are presented in Table 2 and

compared with The semi-analytical solution by Zahedinejad et al. [24] and a 2-D higher-order deformation theory solution by Matsunaga [25]. The material properties in the thickness direction are as bellow:

$$E_i = 70 \text{ (Gpa)} \quad \rho_i = 2702 \left(\frac{\text{kg}}{\text{m}^3} \right)$$

$$E_o = 380 \text{ (Gpa)} \quad \rho_o = 3800 \left(\frac{\text{kg}}{\text{m}^3} \right)$$

$$\nu = 0.3$$

For this simulation, dimensionless first natural frequencies for various thickness to radius ratios and span angles are extracted and listed in Table 3. The comparison is made in this table with the semi-analytical results presented by Zahedinejad et al. [24].

Furthermore, the FG fiber-reinforced cylindrical panel results were obtained and compared with semi-analytical solutions through the differential quadrature method by Yas et al. [29] in Table 4. The fiber and matrix in this example are Tungsten ($E_w = 400 \text{ GPa}$, $\rho_w = 19300 \text{ kg/m}^3$, $\nu_w = 0.28$) and Copper ($E_{cu} = 115 \text{ GPa}$, $\rho_{cu} = 8960 \text{ kg/m}^3$, $\nu_{cu} = 0.31$), respectively, and the volume fractions of the constituent vary according to the power-law distribution from (%100 Cu) at inner to (%25 Cu & %75 W) at outer surfaces. Tables 1, 2, 3, and 4 show an excellent agreement between the results of the present model and other results in the literature. In addition, Table 1 shows that the proposed model has a good convergence rate.

Finally, in this section, the comparison is made for an FG carbon nanotube reinforced panel performed by Yas et al. [30].

In this example, the generalized differential quadrature method derived the normalized natural frequencies of an FG carbon nanotube reinforced panel with SSSS boundary conditions. The frequency parameter is defined as follows:

$$\Omega = 10\omega t \sqrt{\frac{\rho^{CNT}}{E^{CNT}}}$$

Table 1. Fundamental natural frequency parameter for various node distributions, ($L/R_a=0.1$, $L/t=10$ and $\nu=0.3$, $S=R_a\alpha$)

Node distribution ($z \times r \times \theta$)	S/L		
	0.5	1	1.5
30×3×25	1.3175	0.5560	0.4105
40×4×30	1.3172	0.5549	0.4090
45×5×35	1.3171	0.5546	0.4085
50×6×40	1.3170	0.5544	0.4083
[26]	1.3360	0.5563	0.4044
[27]	1.31742	0.55049	0.39987
[28]	1.31597	0.55136	0.40266

Table 2. Fundamental frequency parameters for an (SSSS) FG panel

	n					
	0	0.5	1	4	10	∞
[22]	0.93334	0.8213	0.7483	0.6011	0.5460	0.4752
[21]	0.9187	0.8013	0.7260	0.5797	0.5245	0.4770
Present method	0.9205	0.8017	0.7272	0.5841	0.5322	0.4685

Table 3. Comparison fundamental frequency parameter for an (SSSS) FG panels, ($R_a/L=1$)

	t/R _a			
	$\alpha = \pi/3$		$\alpha = 2\pi/3$	
	0.3	0.5	0.3	0.5
[21]	0.3113	0.6731	0.2279	0.3768
Present method	0.3119	0.6750	0.2265	0.3746

Table 4. Comparison of fundamental frequency parameter for an FG fiber-reinforced cylindrical panel ($L/R_a=1$, $\alpha=\pi/6$, $n=1$)

	R _a /t								
	20	40	60	80	100	120	140	160	180
[26]	0.7530	0.4340	0.3370	0.2930	0.2740	0.2680	0.2620	0.2600	0.2450
Present method	0.7309	0.4259	0.3439	0.3079	0.2923	0.2824	0.2762	0.2720	0.2692

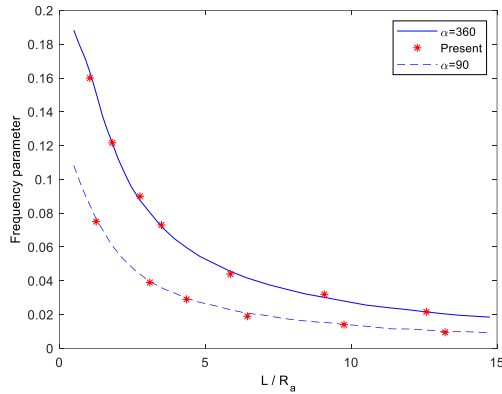


Fig. 3. Comparison of frequency parameter for a CNT reinforced panel ($R_a/t=100, V_{CV}^* = 0.28, FG-V$)

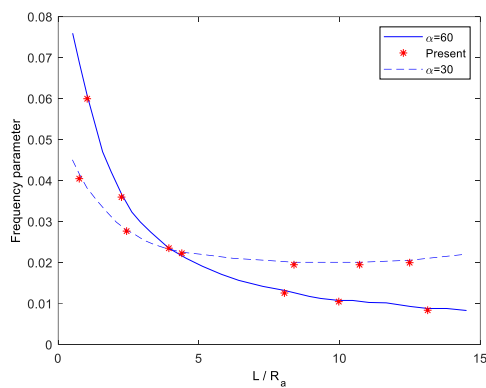


Fig. 4. Comparison of frequency parameter for a CNT reinforced panel ($R_a/t=100, V_{CV}^* = 0.28, FG-A$)

Figures 3 and 4 show the variation of frequency parameters with length to mean radius ratio for an FG – CNT panel for different span angles. It should be noted that the results obtained by the present work are compared with the results of Yas et al. [30]. From figures 3 and 4, it is observed that the present work results are very close to those of Yas et al. [30].

5. Results and Discussion

After validation of numerical results, CNTRC panels are studied by the presented 3D-Mfree simulation. A CNTRC panel is made of Polymethyl-methacrylate (PMMA) like matrix, with CNT as fibers aligned in the axial direction. PMMA is an isotropic material with $E^m = 2.5$ GPa, $\rho^m = 1150$ kg/m³ and $\nu^m = 0.34$. The (10,10) SWCNTs are selected as reinforcements. The material properties of SWCNT are $E_1^{CN} = 5.6466$ TPa, $E_2^{CN} = 7.0800$ TPa, $G_{12}^{CN} = 1.9445$ TPa, $\rho^{CN} = 1400$ kg/m³, and $\nu_{12}^{CN} = 0.175$ [7]. In this work, the CNT efficiency parameters have been estimated by matching Young’s moduli E_{11} and E_{22} of CNTRCs obtained by the rule of the mixture to those from the MD simulations and are listed

in Table 5. Also, the third efficiency parameter is $\eta_3 = 0.7\eta_2$ [7].

The natural frequency parameter is defined as:

$$\bar{\Omega} = \Omega K \sqrt{\rho^m / E^m}$$

Fundamental frequencies of the panel for different span angles are listed in Table 6. This table shows that the maximum and minimum fundamental frequencies are obtained for FG-X and FG- ϕ distribution of CNTs. In the former type, the volume fraction of CNT is zero at the mid surface of the panel and reaches its maximum value at the inner and outer surfaces on which maximum axial deformations occur, while for the latter, one maximum value of CNT volume fraction occurs at the mid surface of the panel, it may justify results obtained from this table. This table also shows that the fundamental frequency of the panel increases slightly with the increase in span angle. Table 7 depicts the effect of the geometry factor, t/R_a , on the first principal frequency of the panel. This table reveals that the fundamental frequency increases with the increase in t/R_a . An increase in this factor means getting thicker and, consequently, stiffer. It can justify the increase of fundamental natural frequency with the increase in t/R_a .

Table 5. Elasticity moduli of PMMA/CNT composites by the rule of the mixture and MD simulation

V_{CV}^*	MD		Rule of mixture			
	E_{11} (GPa)	E_{22} (GPa)	E_{11} (GPa)	η_1	E_{22} (GPa)	η_2
0.12	94.6	2.9	94.78	0.137	2.9	1.022
0.17	138.9	4.9	138.68	0.142	4.9	1.626
0.28	224.2	5.5	224.50	0.141	5.5	1.585

Table 6. First natural frequency parameter for various angle of CCF panel, α . ($t/R_a=0.1, L/R_a=1, V_{CV}^* = 0.17$)

	UD	FG-X	FG-A	FG-V	FG- ϕ
$\alpha=\pi/6$	1.9021	1.9576	1.8004	1.7922	1.7330
$\alpha=\pi/4$	1.9086	1.9629	1.8101	1.8023	1.7350
$\alpha=\pi/3$	1.9088	1.9637	1.8118	1.8022	1.7345
$\alpha=\pi/2$	1.9112	1.9656	1.8140	1.8054	1.7383

Table 7. First natural frequency parameter for panel with various t/R_a ratios. ($L/R_a=2, \alpha=\pi/4, V_{CV}^* = 0.17$)

	h/R_m	UD	FG-X	FG-A	FG-V	FG- ϕ
CCFF	0.01	0.3451	0.3822	0.3215	0.3201	0.3057
	0.05	1.0678	1.2119	0.9333	0.9361	0.8453
	0.1	1.5717	1.6851	1.4234	1.4297	1.3269
	0.2	1.9049	1.9588	1.7917	1.8116	1.7310
CFFF	0.01	0.1206	0.1249	0.1194	0.1195	0.1177
	0.05	0.2608	0.2883	0.2403	0.2414	0.2287
	0.1	0.3894	0.4454	0.3412	0.3445	0.3151
	0.2	0.6161	0.6890	0.5375	0.5444	0.4926

The effects of boundary conditions on the natural frequency parameters are presented in Table 8. According to this table, panels with CCCC and CFFF boundary conditions have the highest and lowest natural frequencies, respectively, as expected. These boundary conditions cause maximum and minimum stiffness values among all boundary conditions listed in this table. Finally, the effects of the volume fraction of CNTs for two boundary conditions are presented in Table 9. This table indicates that all-natural frequencies rise with the increase in volume fraction of CNT. CNT is much stiffer than the matrix material. It justifies the increase of natural frequencies with an increase in volume fraction of CNT. Additionally, it is obvious that for both types of boundary conditions presented in this

table, maximum and minimum values of fundamental frequencies deal with FG-X and FG- ϕ distribution of CNT, but it is not the case for other frequencies.

Table 8. First natural frequency parameter for panel with various boundary conditions. ($L/R_a=1, t/R_a=0.1, \alpha=\pi/3, V_{CV}^* = 0.17$)

	UD	FG-X	FG- Λ	FG-V	FG- ϕ
CCCC	2.3390	2.3987	2.2745	2.2596	2.1998
CCFF	1.9077	1.9637	1.8022	1.8118	1.7345
SSSS	1.5852	1.6958	1.4460	1.4775	1.3724
SSFF	1.4814	1.6039	1.3284	1.3374	1.2308
FFCC	1.3458	1.3740	1.3609	1.3554	1.3410
CFFF	0.6431	0.7132	0.5720	0.5771	0.5270

Table 9. First, five natural frequency parameters for panel with various v^* . ($L/R_a=1, t/R_a=0.1, \alpha=\pi/3$)

			$\bar{\Omega}_1$	$\bar{\Omega}_2$	$\bar{\Omega}_3$	$\bar{\Omega}_4$	$\bar{\Omega}_5$
FFSS	$V_{CV}^* = 0.12$	UD	0.2334	0.3238	0.9982	1.1283	1.4188
		FG-X	0.2413	0.3344	1.0275	1.1605	1.4244
		FG- Λ	0.2353	0.3251	1.0055	1.1349	1.4290
		FG-V	0.2343	0.3251	1.0020	1.1325	1.4179
		FG- ϕ	0.2277	0.3156	0.9771	1.1036	1.4226
	$V_{CV}^* = 0.17$	UD	0.3016	0.4184	1.2895	1.4577	1.8830
		FG-X	0.3177	0.4400	1.3495	1.5236	1.8481
		FG- Λ	0.3056	0.4216	1.3059	1.4726	1.8574
		FG-V	0.3036	0.4215	1.2983	1.4676	1.8356
		FG- ϕ	0.2907	0.4030	1.2497	1.4129	1.8449
	$V_{CV}^* = 0.28$	UD	0.3160	0.4383	1.3510	1.5271	1.9209
		FG-X	0.3537	0.4889	1.4909	1.6812	1.9770
		FG- Λ	0.3262	0.4487	1.3927	1.5688	1.9960
		FG-V	0.3212	0.4478	1.3736	1.5548	1.9512
		FG- ϕ	0.2955	0.4103	1.2757	1.4434	1.9706
CCSS	$V_{CV}^* = 0.12$	UD	1.5336	1.7017	1.8165	2.6248	3.0612
		FG-X	1.5741	1.7071	1.8641	2.6837	3.1335
		FG- Λ	1.4603	1.7022	1.7627	2.6038	2.9348
		FG-V	1.4658	1.7117	1.7673	2.6046	2.9296
		FG- ϕ	1.4093	1.7068	1.7070	2.5409	2.8381
	$V_{CV}^* = 0.17$	UD	1.9605	2.1985	2.3298	3.3806	3.9188
		FG-X	2.0127	2.2143	2.4023	3.4864	4.0108
		FG- Λ	1.8676	2.2045	2.2664	3.3669	3.7617
		FG-V	1.8785	2.2235	2.2744	3.3671	3.7635
		FG- ϕ	1.8070	2.1883	2.2139	3.2617	3.6519
	$V_{CV}^* = 0.28$	UD	2.1056	2.3041	2.4821	3.5656	4.1968
		FG-X	2.1507	2.3675	2.5906	3.7800	4.2903
		FG- Λ	2.0530	2.3460	2.4637	3.6121	4.1161
		FG-V	2.0685	2.3871	2.4682	3.5991	4.1328
		FG- ϕ	2.0225	2.3665	2.3776	3.4352	4.0644

6. Conclusions

Tree-dimensional frequency analysis of FG carbon nanotube-reinforced composite cylindrical panels was carried out by 3D-Mfree simulation. The Galerkin weak forms of governing equations with the platform of the Mfree method are constructed using the Hamilton principle.

The present results are compared with the same results in other works, and it is concluded following results:

1. The 3D-Mfree method has very fast convergence and stability and excellent agreement with the other literature results.
2. The composite panels with the FG-X reinforcement model exhibit the largest fundamental frequency parameters and those of FG-O exhibit the lowest ones.
3. The natural frequencies increase with the increasing volume fraction of CNTs (V_{CN}^*).

References

- [1] Thostenson, E.T., Ren, Z. and Chou, T.W., 2001. Advances in the science and technology of carbon nanotubes and their composites: a review. *Composite Science and Technology*, 61, pp.1899-1912.
- [2] Esawi, A.M.K. and Farag, M.M., 2007. Carbon nanotube reinforced composites: potential and current challenges. *Material and Design*, 28, pp.2394-240.
- [3] Shen, H.S., 2009. Nonlinear bending of functionally graded carbon nanotube-reinforced composite plates in thermal environments. *Composite structure*, 91, pp.9-19.
- [4] Ke, L.L., Yang, J. and Kitipornchai, S., 2010. Nonlinear free vibration of functionally graded carbon nanotube-reinforced composite beams. *Composite Structures*, 92, pp.676-683.
- [5] Sobhani Aragh, B., Nasrollah Barati, A.H. and Hedayati, H., 2012. Eshelby-Mori-Tanaka approach for vibrational behavior of continuously graded carbon nanotube-reinforced cylindrical panels. *Composite Part B: Engineering*, 43, pp.1943-1954.
- [6] Wang, Z.X. and Shen H.S., 2012. Nonlinear vibration and bending of sandwich plates with nanotube-reinforced composite face sheets. *Composite Part B: Engineering*, 43, pp.411-421.
- [7] Moradi-Dastjerdi, R., Foroutan, M. and Pourasghar A., 2013. Dynamic analysis of functionally graded nanocomposite cylinders reinforced by carbon nanotube by a mesh-free method. *Material and Design*, 44, pp.256-266.
- [8] Li, F., and Xiang, Y. 2014. Vibration of carbon nanotube reinforced composite beams based on the first and third-order beam theories. *Applied Mathematical Modelling*, 38(15-16), pp.3741-3754.
- [9] Mehar, K., Panda, S.K. and Mahapatra, T.R., 2017. Theoretical and experimental investigation of vibration characteristics of carbon nanotube reinforced polymer composite structure. *International Journal of Mechanical Sciences*, 133, pp.319-329.
- [10] Karami, B., Shahsavari, D. and Janghorban, M., 2018. A Comprehensive Analytical Study on Functionally Graded Carbon Nanotube-Reinforced Composite Plates. *Aerospace Science and Technology*, 82-83, pp.499-512.
- [11] Zhong, R., Wang, Q., Tang, J., Shuai, C., and Qin B., 2018. Vibration analysis of functionally graded carbon nanotube reinforced composites (FG-CNTRC) circular, annular, and sector plates. *Composite Structures*, 194, pp.49-67.
- [12] Bouazza, M. and Zenkour, A.M., 2020. Vibration of carbon nanotube-reinforced plates via refined nth-higher-order theory. *Archive of Applied Mechanics*, 90, pp.1755-1769.
- [13] Demir, Ç. and Civalek, Ö., 2017. On the analysis of microbeams. *International Journal of Engineering Science*, 121, pp.14-33.
- [14] Jalaei, M.H. and Civalek, Ö., 2019. On dynamic instability of magnetically embedded viscoelastic porous FG nanobeam. *International Journal of Engineering Science*, 143, pp.14-32.
- [15] Civalek, Ö., Dastjerdi, S., Akbas, S.D. and Akgöz, B., 2021. Vibration analysis of carbon nanotube-reinforced composite microbeams. *Mathematical Methods in the Applied sciences*, Doi: 10.1002/mma.7069.
- [16] Zeverdejani, M.K. and Beni, Y.T., 2020. Effect of laminate configuration on the free vibration/buckling of FG Graphene/PMMA composites. *Advances in Nano Research*, 8(2), pp.103-114
- [17] Zeverdejani, M.K., Beni, Y.T. and Kiani, Y., 2020. Multi-Scale Buckling and Post-Buckling Analysis of Functionally Graded Laminated Composite Plates Reinforced by Defective Graphene Sheets. *International Journal of Structural Stability and Dynamics*, 20(1), 2050001.
- [18] Zeverdejani, M.K. and Beni, Y.T., 2019. Size-dependent vibration analysis of graphene-PMMA lamina based on non-classical continuum theory. *Science and Engineering of Composite Materials*, 26, pp.491-501.
- [19] Zhu, P., Lei, Z.X. and Liew, K.M., 2012. Static and free vibration analyses of carbon

- nanotube-reinforced composite plates using finite element method with first-order shear deformation plate theory. *Composite structure*, 94, pp.1450-1460.
- [20] Reddy, J.N., 1945. *Mechanics of laminated composite plates and shells: theory and analysis*, 2nd ed. CRC Press.
- [21] Soltanmaleki, A., Foroutan, M. and Alihemmati J., 2016. Free vibration analysis of functionally graded fiber reinforced cylindrical panels by a three-dimensional mesh-free model. *Journal of Vibration and Control*, 22(19), pp.4087-4098.
- [22] Alihemmati, J., Foroutan, M. and Soltanmaleki, A., 2017. Dynamic analysis of functionally graded fiber reinforced cylinders under an impact load by a three-dimensional mesh-free approach. *Journal of the Dynamic Behavior of Materials*, 3(3), pp.391-406.
- [23] Liu, G.R., 2003. *Mesh free methods: moving beyond the finite element method*, CRC Press.
- [24] Zahedinejad, P., Malekzadeh, P., Farid M. and Karami G., 2010. A semi-analytical three-dimensional free vibration analysis of functionally graded curved panels. *International Journal of Pressure Vessels and Piping*, 87, pp.470-480.
- [25] Matsunaga H., 1999. Vibration and stability of thick simply supported shallow shells subjected to in-plane stresses. *Journal of Sound and Vibration*, 225(1), pp.41-60.
- [26] Kobayashi, A.W. and Leissa, A.W., 1995. Large amplitude free vibration of thick shallow shells supported by shear diaphragms. *International Journal of Non-Linear Mechanics*, 30, pp.57-66.
- [27] Chern, Y.C. and Chao, C.C., 2000. Comparison of natural frequencies of laminates by 3-D theory, Part II: curved panels. *Journal of Sound and Vibration*, 230(5), pp.1009-1030.
- [28] Yang, J. and Shen, H.S., 2003. Free vibration and parametric resonance of shear deformable functionally graded cylindrical panels. *Journal of Sound and Vibration*, 26, pp.871-893.
- [29] Yas, M.H., SobhaniAragh, B. and Heshmati, M., 2011. Three-dimensional free vibration analysis of functionally graded fiber reinforced cylindrical panels using differential quadrature method. *Structural Engineering and Mechanics*, 37(5), pp.529-542.
- [30] Yas, M.H., Pourasghar, A., Kamarian, S., and Heshmati, M., 2013. Three-dimensional free vibration analysis of functionally graded nanocomposite cylindrical panels reinforced by carbon nanotube. *Materials and Design*, 49, pp.583-590.